IEEE Robotics and Automation Letters (RA-L) paper, presented at ICRA 2026, Vienna, Austria. Cite as RA-L paper.

Architected Vacuum Driven Origami Structures via Direct Ink Writing of RTV Silicone

Qiyao Wang[1], Thileepan Stalin[1] and Pablo Valdivia y Alvarado[1,2,3]

***Abstract*—Recent advances in soft robotics, wearable devices, and deployable systems have sparked tremendous interest in origami structures due to their controllable volume changes and shape-morphing capabilities. Despite significant progress in the design and fabrication of origami using traditional materials such as paper, textiles, thermoplastics, and thick panels, challenges persist in creating soft elastomeric origami designs that allow for precise, programmable deformations. This work proposes an architected approach for designing and 3D printing Room Temperature Vulcanization (RTV) silicone-based origami structures actuated by negative pressure. Central to this approach is a flexible hinge design, which enables controlled bending angles ranging from 45° to 90° upon the application of vacuum actuation. This architected method simplifies the complex folding of origami structures by strategically arranging the flexible hinges. A Python-based software tool was developed to generate custom G-code directly from user-defined design parameters, streamlining the design-to-fabrication pipeline for Direct Ink Writing (DIW) RTV silicone-based origami parts. Initial fabrication experiments were conducted using a three-step print-assemble-bond approach. As an alternative to eliminating manual processing steps, a monolithic flexible hinge with a cavity was printed within a gel support. This paper introduces a hinge design library and discusses the design-to-fabrication workflow for origami-inspired active structures.**

***Index Terms*—Architected Materials, DIW, Silicone Origami, Soft Robotics.**

I. INTRODUCTION

RECENT advancements in soft robotics, wearable devices, and 3D printing have ignited interest in traditional art forms like Origami and Kirigami within the research community [1], [2]. Drawing inspiration from origami, numerous research groups have developed shape-morphing structures [3], [4]. Traditional materials like paper, textiles, thermoplastics and thick panels are widely used to create origami structures [5]–[7]. The ability to transform shapes through meticulously designed crease patterns makes these structures ideal for adaptable and deployable applications. Origami-based actuators and manipulators, in particular, hold great promise due to their safety, shape-morphing capabilities and their ability to adeptly manipulate objects of varying shapes and sizes [8], [9]. Origami-inspired structures have also been studied for biomedical applications as they can change shape and size, making them ideal for various applications [10], [11]. In addition, origami-inspired designs are revolutionising the development of metamaterials, enabling tunable mechanical properties and distinctive characteristics [12], [13].

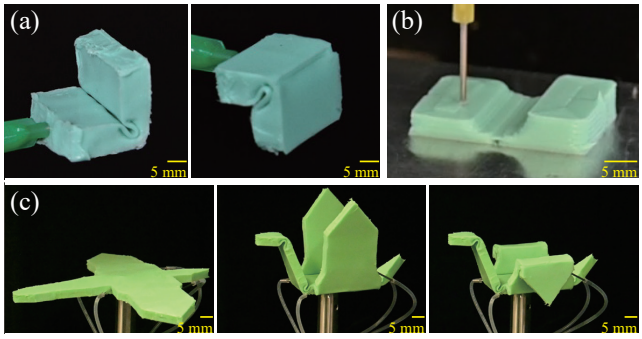

Fig. 1. a) Image of a 90° hinge in bent state. b) DIW 3D Printing the base of a 90° hinge. c) Demonstration of an actuated origami flapping bird in three distinct states.

Appropriate actuation mechanisms are key to realize and implement origami structures. Embedded motors provide precise and robust actuation, and are suitable for large structures [14]. Cable-driven actuators offer simplicity and large deformation capabilities, but cable management and potential slack issues should be considered [15], [16]. Shape memory materials enable remotely controlled deformation via thermal or electrical stimulation [17], [18]. Electromagnetic actuation uses magnetic fields for remote actuation and is particularly applicable to wireless medical devices [10], [19]. Pneumatic actuation uses positive air pressure or vacuum to generate large forces and deformations [20], [21]. However, integrating these actuation methods in soft origami structures presents challenges in terms of fabrication complexity, rapid actuation, and flexible deployment. Pneumatic actuation stands out due to its potential for rapid response, large deformation, design flexibility, and adaptability (e.g., water resistance). Despite these advantages, pneumatic structures often have large, complex air channels to apply air pressure or vacuum. The design and fabrication of origami structures with integrated air channels for reliable programmable folding remains an area for further research.

Manuscript received: April 30, 2025; Accepted: June 26, 2025.

This paper was recommended for publication by Editor Cecilia Laschi upon evaluation of the Associate Editor and Reviewers' comments.

This research was supported by grants from the National Research Foundation, Prime Minister's Office, Singapore under its Campus of Research Excellence and Technological Enterprise (CREATE) programme, and by A*STAR under RIE2025 Manufacturing, Trade And Connectivity (MTC) Programmatic Fund. Grant No: M24N3b0028.Title: 4D Additive Manufacturing (4DAM) of Smart Structures.

[1]EPD, Singapore University of Technology and Design, Singapore.

[2]SUTD Digital Manufacturing and Design (DManD), Singapore.

[3]Singapore-HUJ Alliance for Research and Enterprise (SHARE), The Smart Grippers for Soft Robotics (SGSR) Programme, Campus for Research Excellence and Technological Enterprise (CREATE), Singapore 138602.

[†]Corresponding Author: pablov@sutd.edu.sg

Digital Object Identifier (DOI): see top of this page.

IEEE Robotics and Automation Letters (RA-L) paper, presented at ICRA 2026, Vienna, Austria. Cite as RA-L paper.

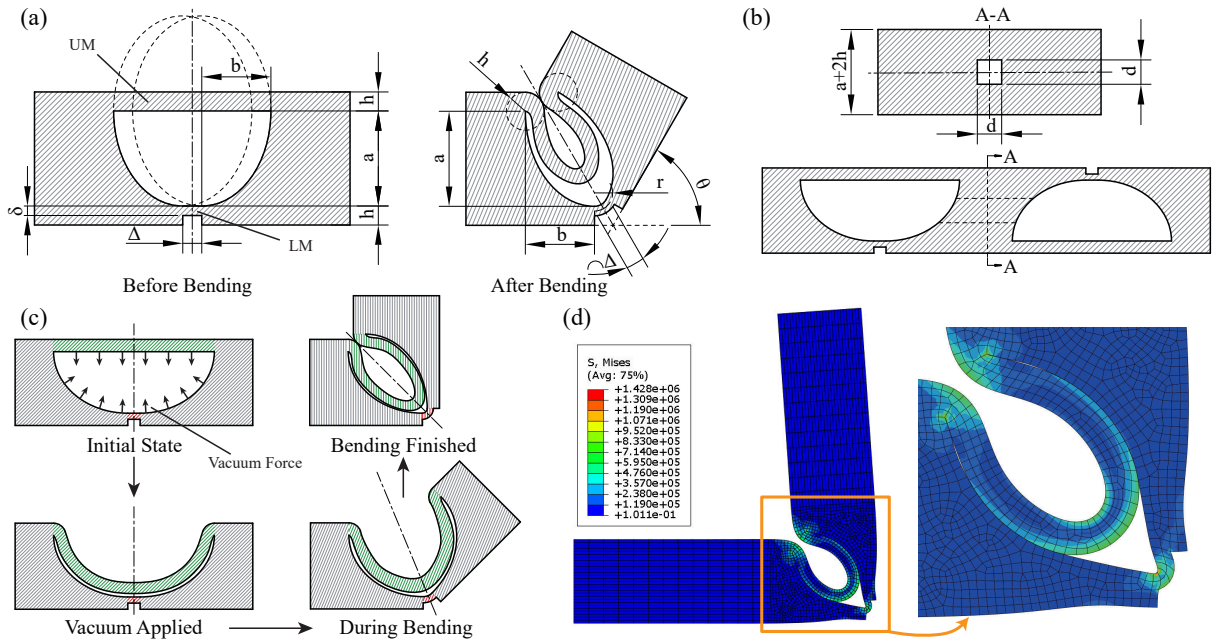

Fig. 2. a) Illustration showing cross-sectional views of a generic hinge at both its initial and bent states. The internal cavity is shaped by two-quarter ellipses separated by a small rectangular gap. The thickness of the lower hinge membrane (LM) is reduced to facilitate bending. The length of the ellipse's two axis, a and b, determines the required final bending angle θ under two assumptions: The length of LM, Δ, is considered constant during bending, and it stops bending when contact occurs at the top of the hinge. b) Cross-sectional views of two hinges connected by an air channel (see detail A-A). c) Illustrations showing a hinge bending sequence. The initial shape change is caused by vacuum, and the following shape changes are driven by strain energy exchange between different parts of the hinge. d) The simulation result of a bent 90° hinge with the visualization of von Mises stress.

Origami traditionally requires a time-consuming manual folding process and memorization of crease patterns. However, the advent of digital fabrication tools assisted researchers to explored automated alternatives to streamline these tasks. Advances in 3D printing technologies have greatly aided the fabrication of shape-morphing structures. Among various soft materials that can be used for such structures, RTV silicone stands out due to its flexibility, stretchability, and durability. Direct ink writing (DIW) of silicone is a rapidly growing method that simplifies the design and fabrication process, making it easier to realize more complex and integrated structures [22]–[24]. Furthermore, technologies such as freeform liquid 3D printing (FL3DP) and in-situ freeform liquid 3D printing (iFL3DP) facilitate the fabrication of complex structures featuring intricate cavities and cantilevers [25], [26]. The biggest challenge is creating printable models and fabrication files from complex origami designs. Another major concern is the development of integrated actuation mechanisms, such as vacuum channels and precise control of flexible hinges for various geometries and materials.

Existing slicers such as Cura, PrusaSlicer, and OctoPrint generate G-code files based on CAD files more suitable for FDM 3D printers [27], [28], [29]. The slicer-generated toolpaths have print moves and excessive travel moves, which can cause toolpath jerks. FDM printers are unaffected by these toolpath jerks, thanks to instant-curing thermoplastics. However, these slicer-generated toolpaths are unsuitable for slow-curing RTV silicones, as the printed structure may collapse due to small jerks.

In this paper, we propose an architected approach to design and 3D print silicone origami structures (see Fig.1). Flexible hinges can be designed to bend from 45° up to 90° upon vacuum actuation. These flexible hinges can be carefully arranged to construct complex origami structures. Vacuum actuation was chosen for this work because of its safety and ability to produce rapid, large deformations. In addition, a Python-based tool was developed to streamline the design-to-fabrication workflow, enabling users to easily generate 3D printable models with customised origami patterns. The main contributions of this paper are summarized below:

1) Flexible hinge design library with various bending angles for vacuum actuation.
2) A Python-based software tool to streamline the design-to-fabrication workflow.
3) Fabrication of various origami structures with flexible hinges using either multi-step DIW or single-step FL3DP printing methods.

II. Design

This section details the design considerations of the proposed flexible hinge for origami structures. A flexible hinge is a simple and efficient way to achieve bending motions for origami structures [30]. Geometry and material distribution dictate a hinge's bending behaviour. The proposed hinge design considers three principles:

1) Minimal hinge thickness.
2) Geometrical defined bending limits.
3) 3D printable designs.

The hinge cross-section shown in Figure 2a. consists of a symmetric cavity design to control bending under vacuum

IEEE Robotics and Automation Letters (RA-L) paper, presented at ICRA 2026, Vienna, Austria. Cite as RA-L paper.

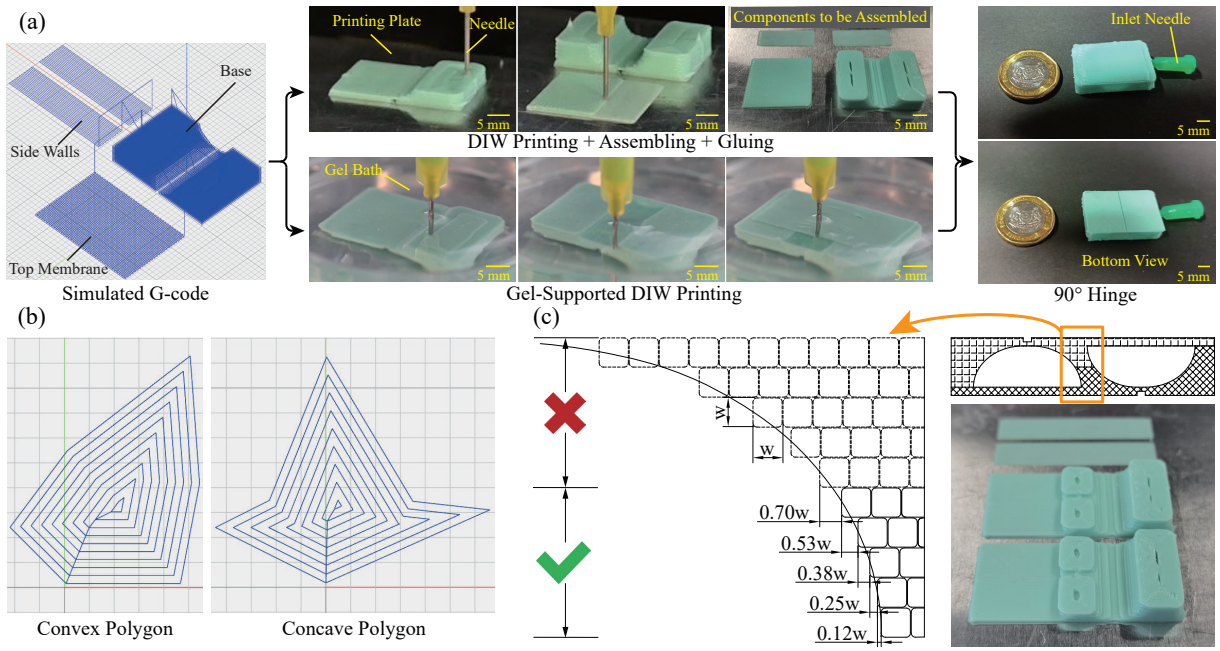

Fig. 3. a) Design-to-fabrication workflow. G-code can be generated to fabricate origami structures either by the print-assemble-glue method or by directly printing a monolithic structure using gel support. b) Two images show the simulated toolpath for CPO concentric infill pattern. c) Illustration shows the load distribution on an overhanging structure and the printing strategy by segmenting the complex overhangs for DIW process.

actuation. The cavity consists of two quarter ellipses mirrored about the hinge's axis, with a small rectangular channel between them. This geometry allows bending by concentrating deformation on one side of the hinge. Vacuum application significantly deforms the thin upper membrane (UM, also highlighted in green in Fig. 2c) due to the pressure difference, and the narrow lower membrane (LM, also highlighted in red in Fig. 2c) on the other side acts as the hinge point (see Fig. 2c). The U-shaped cavity accommodates UM's downward deflection, preventing premature self-contact of UM which may block the bending [21]. The values for the design parameters shown in Figure 2a are listed in Table 1. The ellipse's minor radius b is determined based on the desired bending angle θ.

The hinge's bending process (see Fig. 2c) can be broken down into three distinct stages: i) initial vacuum-induced deformation, ii) strain energy-driven rotation, and iii) geometric blocking. Vacuum pulls UM downwards, stretching it to touch the cavity base. This deformation stores the strain energy in UM, which tries to minimise this energy by shortening; therefore, the structure bends around its weakest point, the lower hinge point. The bending stops when contact is made at the top of the hinge on both sides.

During bending, strain energy decreases in UM while increasing in the LM. Without considering geometric constraints, bending stops at an angle where the total strain energy is minimized. To comply with the second design principle, this theoretical energy minimum is supposed to occur at a sufficiently large bending angle larger than the desired bending angle. That way, the bending will stop because of the contact of the hinge's both sides, instead of reaching an equilibrium bending angle before the geometrically defined angle. Therefore, LM should be relatively thin to reduce the energy required for bending [31]. Additionally, the geometrical parameters of LM should be carefully controlled to prevent snap-through.

TABLE 1
HINGE GEOMETRICAL PARAMETERS

variable	bending angle	value
a		4.00 mm
h		0.80 mm
Δ		0.80 mm
δ		0.40 mm
d		1.60 mm
	90°	4.82 mm
b	60°	2.91 mm
	45°	2.19 mm

A finite element analysis (FEA) simulation of a 90° hinge (see Fig. 2d) showed that it is essential to have a thin LM. This design makes bending easier and ensures that the bending is centered around the hinge point, contributing to the final bending angle. The FEA simulations were performed with Abaqus using the elastic model and C3D8R quadratic elements, and fixed constraints were applied at the leftmost edge. An inward uniform load is added on the cavity boundary to simulate vacuum pressure.

The relationship between the parameters is determined geometrically when bending terminates (see Fig. 2b). Two key assumptions are made:

1) Bending stops when the vertices on both sides of the hinge come into contact. UM's local deformed shape can be approximated as a circular arc with a radius equal to its thickness h.
2) The centerline length of LM remains constant as Δ

IEEE Robotics and Automation Letters (RA-L) paper, presented at ICRA 2026, Vienna, Austria. Cite as RA-L paper.

TABLE 2
DESIGN TO FABRICATION TIME DETAILS

Sample	G-code Generation	3D Printing	Curing	Assembly	Final curing	Total	Manual Post-Process
Single hinge	$<$ 2 s	8 min	20 min	$<$ 5 min	20 min	$<$ 53 min	$<$ 13 min
Origami cube	$<$ 2 s	32 min	20 min	$<$ 10 min	20 min	$<$ 82 min	$<$ 42 min
Origami bird	$<$ 2 s	64 min	20 min	$<$ 20 min	20 min	$<$ 124 min	$<$ 84 min

during bending. This assumes that the deformation of the lower membrane is only bending.

The relationship between b and θ can be expressed by Eq. 2. Numerical values for b for three different angles are also listed in Table 1.

$$r = \frac{\Delta}{\theta} \tag{1}$$

$$b(\theta) = a\ \tan\frac{\theta}{2} + \frac{1}{\cos\frac{\theta}{2}}[h - (r - \frac{\delta}{2})\ \sin\frac{\theta}{2}] \tag{2}$$

A network of interconnected air channels was designed to enable the simultaneous actuation of multiple hinges within a single origami structure. Figure 2b shows the cross-section of the air channel connecting two neighbouring hinges. This interconnected network of air channels ensures a uniform pressure distribution across the structure, resulting in synchronised actuation of the origami structure.

Additionally, to ensure the cavity remains sealed, side walls are added on both sides of the hinge. To minimize bending stress, the wall thickness is reduced and set to the printing line width (0.4 mm).

III. FABRICATION

Flexible silicone hinge based origami structures were 3D printed and actuated using negative pressure (see Fig. 3a). The flexible hinge structures were fabricated either by the print-assemble-glue method (i.e DIW + assembly) or by directly printing a monolithic origami structure using support gels (i.e. FL3DP). Finally, a tube or a stainless steel needle was inserted into the structure inlet port, connecting it to a vacuum pump for actuation.

A. 3D-Printing G-code Auto-Generation

A Python-based tool was developed to allow the user to define the base geometry and hinge parameters and auto-generate the G-code for 3D printing. Each part of the proposed structure can be abstracted as a frustum, enabling a layer-by-layer printing strategy. Regardless of the structure's complexity (single hinge or composite origami structure), each layer is composed of one or more polygons. The edges of the polygons define the hinges and shape contours, so it is important to ensure the print quality of the edges. Therefore, contour-parallel offset (CPO) was used to efficiently generate concentric infill patterns for these polygons [32]. This pattern is generated through a series of iterative steps:

1) Contour tracing: The pattern begins by tracing the outermost perimeter of the polygonal layer.

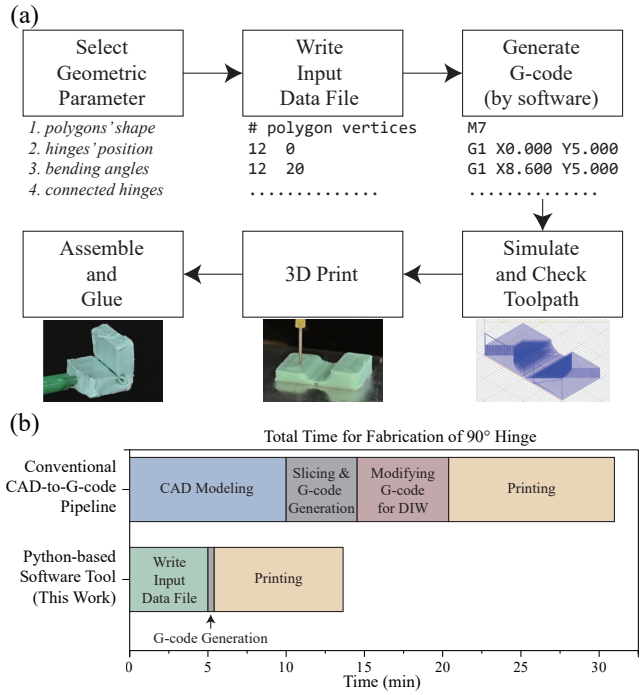

Fig. 4. a) Flowchart highlighting the design-to-fabrication workflow. b) The plot compares the total time taken to fabricate a 90° hinge, excluding the time costs for curing, assembling, and gluing, using both a conventional CAD-to-G-code pipeline and a Python-based software tool developed (this work).

2) Parallel Offset: Each edge of the initial polygon is offset inwards by a fixed distance equivalent to the width of the printed line, creating a smaller polygon.
3) Iteration: Steps 1 and 2 are repeated until the remaining interior area becomes too small for further offsets.

Figure 3b presents two representative examples of CPO infill patterns: one convex and one concave polygon. These examples demonstrate the method's efficiency in generating infill patterns for various geometric configurations. This strategy also promotes continuous toolpaths with minimal extrusion start and stops, further enhancing printing quality.

An alternating in-out printing strategy was also implemented to create a continuous toolpath. In odd-numbered layers, the toolpath moves from the outer perimeter to the center in a counterclockwise direction, while in even-numbered layers, it moves clockwise from the center to the perimeter. This ensures continuous tool paths and minimizes prolonged shear stress on bottom layers. Additionally, to avoid over-extrusion in narrow zones, infill polygon offsetting stops when the point spacing falls below the printing line width.

A few origami design software packages [33], [34] are available to design and simulate origami structures; this proposed

IEEE Robotics and Automation Letters (RA-L) paper, presented at ICRA 2026, Vienna, Austria. Cite as RA-L paper.

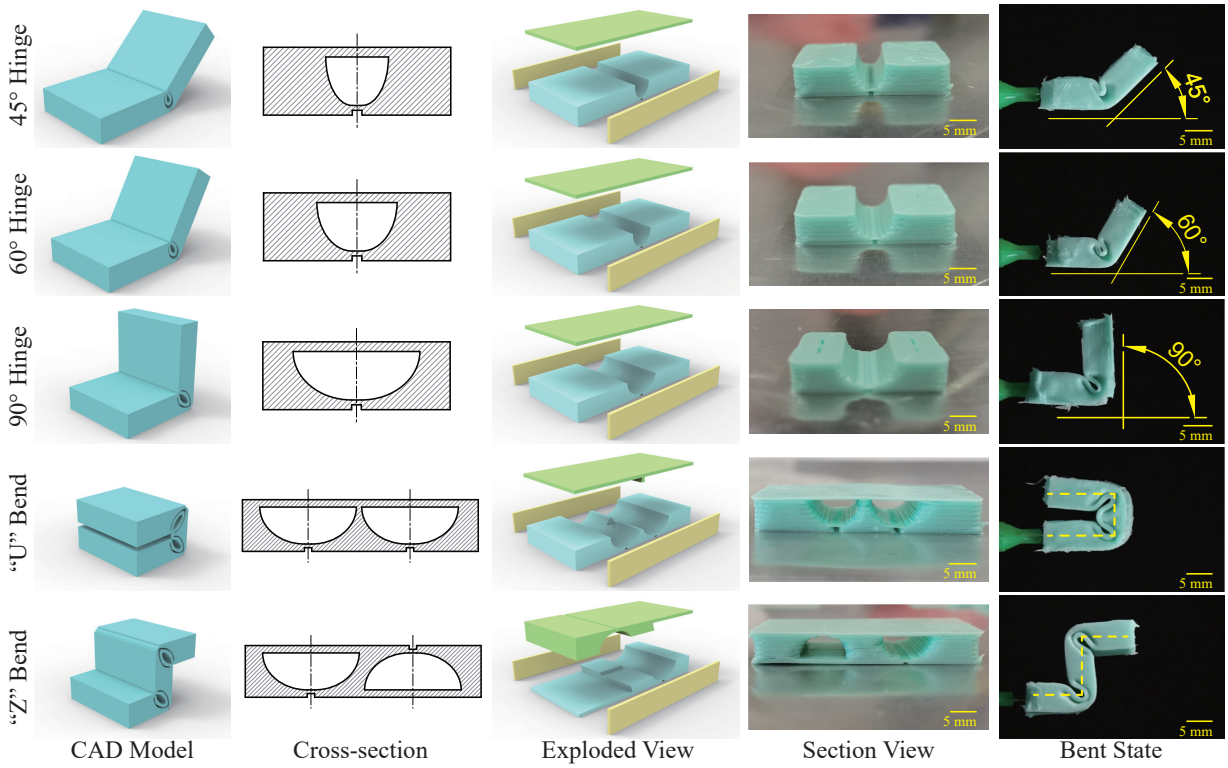

Fig. 5. Multiple views showcasing a variety of flexible hinge designs. Columns from left to right show: CAD models, cross-sectional views, assembly exploded views, printed hinge base structures without walls, and actuated prototypes in fully bent states.

tool focuses specifically on generating optimal G-code from user inputs for 3D printing. The tool accepts the geometric information about an origami structure as an input to generate a ready-to-print G-code. (see Fig. 4 and Fig. 7a, 7b). The process begins by defining the vertices for the base origami shape. Next, the user specifies the polygon edges, which function as hinges. The user then inputs the bending information for each hinge, which includes the target folding angle and the desired folding direction (e.g., valley fold (VF) or mountain fold (MF)). Finally, the user labels groups of hinges requiring synchronous actuation (connected hinges, CH), allowing the program to generate the corresponding connecting air channel networks automatically.

The entire process, from the user input to the final fabricated structure for the two demonstrations is shown in Figure 4a. Based on the user's design inputs, the program automatically creates 3D-printable G-code in the "Generate G-code" step. The proposed Python-based tool generates G-code files for the bottom part, top part, and sidewalls for the print-assemble-glue method. To make room for the hinges, the computer program first slightly offsets each polygon. The base layers are then formed by drawing the overall structure's outer contour. The tool then determines the frustum shapes derived from each polygon, defining the polygons for each printing layer, and computes the hinge geometries based on the design functions and user inputs. Following the creation of air channels, the corresponding polygons in the middle layers are subdivided to create the upper and lower frustums. Each layer's toolpaths are created appropriately and combined. Lastly, the number and location of hinges are used to create the sidewall toolpaths. Before printing, the generated toolpaths can be simulated using online simulation tools like NC-Viewer [35] to make sure the generated G-code files are correct. The total time required to design and fabricate a 90° hinge using a Python-based software tool (this work) and a traditional CAD-to-G-code pipeline was calculated. Figure 4b illustrates the total time required from design to fabrication for both methods. The traditional method requires CAD modelling followed by slicing, resulting in a G-code file primarily suited for FDM 3D printers. These G-code files need modification before they can be utilised for silicone 3D printing, which includes adding start and stop pressure signals for extrusion. In the proposed workflow, the user no longer needs to perform CAD modelling for all components; instead, the tool accepts the geometric information of origami structures as a text file. The proposed tool generates G-code files for silicone 3D printing with optimal print paths and fewer non-print moves, thus achieving a better finish while reducing printing time.

B. Silicone 3D Printing

The flexible hinge origami structures can be fabricated either by the print-assemble-glue method (i.e. DIW + assembly) or by directly printing a monolithic origami structure using support gels (i.e. FL3DP). In the print-assemble-glue method, DIW was used as a printing method. DIW of RTV silicones with overhanging structures and cavities is challenging without the use of sacrificial support. To address this, toolpaths must be carefully segmented to accommodate the internal cavities

IEEE Robotics and Automation Letters (RA-L) paper, presented at ICRA 2026, Vienna, Austria. Cite as RA-L paper.

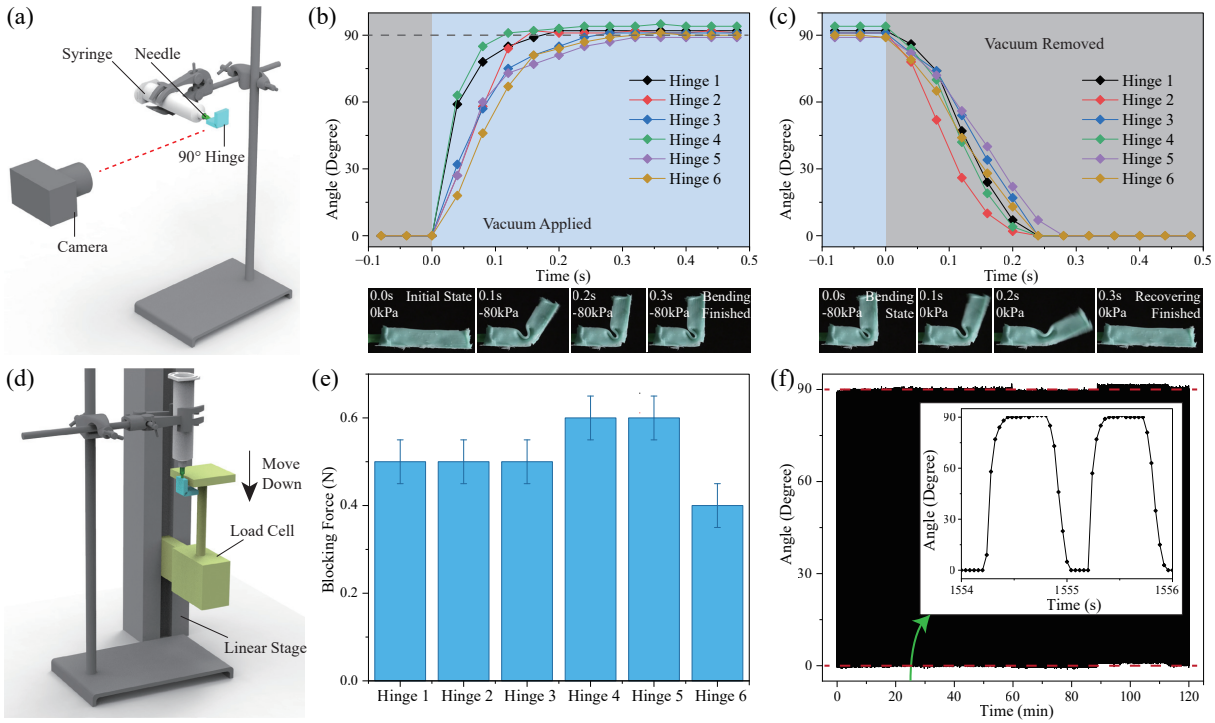

Fig. 6. a) CAD drawing of the experimental setup used to characterize hinge bending. b) Bending response vs. time for six 90° hinges fabricated using the print-assemble-glue method during Vacuum ON (-80kPa) state. c) Bending recovery response vs. time for six 90° hinges fabricated using the print-assemble-glue method during Vacuum OFF state. d) CAD drawing of the experimental setup used to measure hinge blocking force. e) Blocking force vs. time for the six hinges tested. f) Cyclic bending test of a hinge operating at 1 Hz for two hours. The hinge operates robustly for the entire test duration indicating the structure durability.

of the hinge. Therefore, hinge structures were split into four components easily fabricated via conventional DIW: a base, a top membrane, and two side walls and then assembled (see Fig. 3a and Fig. 5). The top membrane requires a high Young's modulus, and to ensure simplified fabrication, Smooth-Sil 960 (purchased from Smooth-On, USA, $E_{100\%} = 1.93$MPa) was used for all components. The printing line width and layer height were set to 0.4 mm. After curing, the printed parts were assembled and glued using Sil-Poxy adhesive (Smooth-On, USA). A single hinge (30 mm x 20 mm) required approximately 6 minutes to print and 2 minutes to assemble (excluding curing time).

DIW of overhanging structures without support is challenging and prone to collapse due to sagging. When fabricating complex structures with multiple hinges, certain geometric configurations require printing some hinges components in an inverted orientation, with the wider cavity opening facing downward. A 90-degree hinge structure, which displays a maximum overhang, is used as an example (see Fig. 3c). The first five layers have a controlled overhang (smaller than 50% of printing line width) and can be printed without any support. However, the later layers exceed the printable limit. Therefore, the hinge is divided into two parts (shown with two different crosshatching patterns in Fig. 3c): the bottom half of the layers are printed together upward, and the remaining half is printed in the reverse direction as another part.

In addition to the multi-step fabrication approach, a single-step fabrication method with gel support was explored. This method allows the entire hinge with cavities to be printed as a single monolithic unit, eliminating the need for a manual assembly process. The support gel on the exterior surface can be washed with water [26], and a syringe can be used to remove the gel trapped in the inner cavity. However, printing inside a gel support requires careful selection of print parameters, especially the printing speed. Rapid movements can disturb the support gel and affect printing accuracy. In our experiments, it took about 20 minutes to fabricate a single hinge (30 mm x 20 mm), much longer than the DIW method. Single-step fabrication has many advantages, but the long curing time inside the gel and the slow printing speed must be further optimized to decrease the total fabrication time. Table 2 summarizes the time required to fabricate each hinge and two demonstration structures. The time taken for G-code generation, printing, and assembly of different parts was recorded. Excluding the silicone curing time, a single hinge can be fabricated in under 13 minutes, while a complex origami structure, such as an origami bird, can be completed in less than 90 minutes.

IV. Results

In this section, the proposed flexible hinge structures are validated through demonstrations and characterization tests.

Figure 5 illustrates various primitive hinge designs with various bending angles that can be combined to form more complex structures. Five different primitive hinges are shown:

1) A 45° hinge.

IEEE Robotics and Automation Letters (RA-L) paper, presented at ICRA 2026, Vienna, Austria. Cite as RA-L paper.

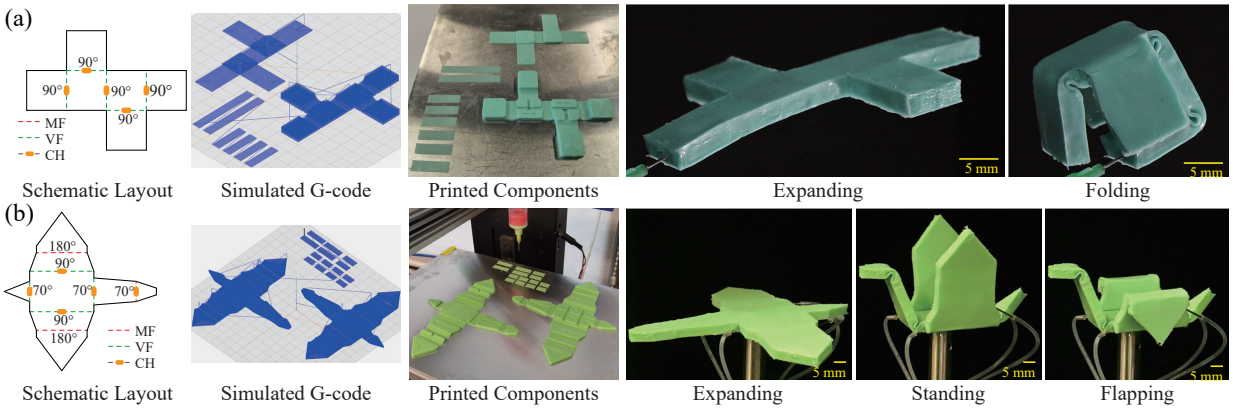

Fig. 7. Schematic layout (based on user input),images show toolpath simulation, printing process, and working prototype: a) An origami cube; b) An origami flapping bird.

2) A 60° hinge.
3) A 90° hinge.
4) A ”U” hinge assembly: integrating two 90° hinges oriented in the same direction, enabling a combined bending angle of 180°.
5) A ”Z” hinge assembly: integrating two 90° hinges oriented in the opposite direction, achieving a zigzag folding pattern.

Figure 5 shows the CAD models of various hinges, cross-sectional views, exploded views of the structure assemblies, views of the printed bases without walls, and prototypes in fully bent states for each hinge type.

A series of mechanical characterization experiments were conducted to determine the performance of the fabricated flexible hinge structures including 1) actuation and recovery response, 2) blocking force of bending state and 3) working durability. Six identical 90° hinges were fabricated using the print-assemble-glue method and then subjected to bending tests to assess the reproducibility of performance with this fabrication approach.

Figure 6a shows the experimental setup used to record the bending behaviour of the flexible hinges. A side view video was recorded of the vacuum-actuated bending motion for each horizontally mounted hinge. The video was then processed using OpenCV to extract quantitative data on the hinge bending angle over time. The actuation and recovery responses of the six hinges to the vacuum ON (-80kPa) and OFF cycle are shown in Figures 6b and 6c respectively. The results confirm that the hinges exhibit fast bending and recovery cycles. The average time needed to complete the bend was 0.22s with a standard deviation of 0.07s, and the average restoring time was 0.28s with a standard deviation of 0.04s, which reflects the ability of the hinges to deform quickly. The six hinge samples characterized for response times demonstrated minimal variation, highlighting the reproducibility of the fabrication process.

Figure 6d shows the experimental setup used to measure the blocking force, a crucial parameter for applications involving interaction with external loads, of a 90° hinge. A slide rail and a load cell were used to measure the forces. The contact point of the load cell's head with the hinge is maintained at a horizontal distance of 1 cm from the structure's hinge point, and the platform with the load cell moves downwards. Figure 6e shows the measured blocking forces for six 90° hinges. The peak blocking forces were consistently around $0.5N$, further confirming the reliability and reproducibility of the manufacturing process.

Finally, a continuous cyclic test was conducted to evaluate the durability of the hinges (see Fig. 6f). During this experiment, a 90° hinge was subjected to a bend-recover cycle at a frequency of 1 Hz for a period of two hours of continuous operation (a total of 7,200 cycles). The hinge's maximum and minimum bending angles remained almost constant throughout the experiment, indicating the hinge's robustness and stable operational performance. The Abaqus FEA simulation (see Fig. 2d) shows that the maximum stress of a bent 90° hinge (1.43MPa) is within the material's tensile strength (4.48MPa), contributing to a long service life.

Together, these results shows that the proposed hinge design is highly suitable for dynamic origami applications due to its rapid response, robustness, and high reproducibility.

Two functional origami demonstrations, a expanding-folding cube and an origami flapping bird, were fabricated to illustrate the effective use of the proposed design approach, fabrication methods, and software tool. The geometric parameters of the hinges used in both demonstrations are listed in Table 1. According to the complete design-to-fabrication workflow shown in Figure 4a, Figure 7a shows details for the origami cube, starting with a schematic layout of user-defined input, then a simulated G-code visualized by NC-viewer, and then the structure's initial and bending states. Similarly, Figure 7b shows details for the flapping bird, which has a more complex structure with two independent actuation sections and three operating states.

V. Conclusion

This work demonstrated a flexible hinge design with programmable bending angles to create complex morphing structures. This streamlined design-to-fabrication approach allows for customizable designs. Mechanical characterisation results are promising, showing rapid bending-recovery cycles and long-term durability. Despite this promising performance,

IEEE Robotics and Automation Letters (RA-L) paper, presented at ICRA 2026, Vienna, Austria. Cite as RA-L paper.

some limitations exist in designing and fabricating thin hinge structures. The fabricated flexible hinge is 5.6 mm thick, and 4.8 mm is the minimum thickness fabricated so far. Scaling down the thickness of the hinge requires reduced geometries and thin membranes, which may lead to insufficient bending angles. Future studies will focus on improving structural design, optimizing printing toolpath, and exploring more suitable materials to realize paper-like origami units with minimum thickness. Due to geometric limitations and complexity, the current design does not permit cross-folding [36]. Future studies will also investigate design and fabrication strategies for complex folding patterns with thin functional hinges. This work has enormous potential for reconfigurable soft robots, deployable structures, and wearables.

APPENDIX

The Python code with examples of this work can be found at https://github.com/SUTD-BRDLab/Architected-Origami

REFERENCES

[1] A. Rafsanjani, Y. Zhang, B. Liu, S. M. Rubinstein, and K. Bertoldi, "Kirigami skins make a simple soft actuator crawl," *Science Robotics*, vol. 3, no. 15, p. eaar7555, 2018.

[2] Q. Ze, S. Wu, J. Nishikawa, J. Dai, Y. Sun, S. Leanza, C. Zemelka, L. S. Novelino, G. H. Paulino, and R. R. Zhao, "Soft robotic origami crawler," *Science advances*, vol. 8, no. 13, p. eabm7834, 2022.

[3] S. Zhang, X. Ke, Q. Jiang, H. Ding, and Z. Wu, "Programmable and reprocessable multifunctional elastomeric sheets for soft origami robots," *Science Robotics*, vol. 6, no. 53, p. eabd6107, 2021.

[4] A. Kotikian, C. McMahan, E. C. Davidson, J. M. Muhammad, R. D. Weeks, C. Daraio, and J. A. Lewis, "Untethered soft robotic matter with passive control of shape morphing and propulsion," *Science robotics*, vol. 4, no. 33, p. eaax7044, 2019.

[5] S. Alharbi, S. Chaudhari, A. Inshaar, H. Shah, C. Zou, R. L. Harne, and A. Kiourti, "E-textile origami dipole antennas with graded embroidery for adaptive rf performance," *IEEE Antennas and Wireless Propagation Letters*, vol. 17, no. 12, pp. 2218–2222, 2018.

[6] S. Townsend, R. Adams, M. Robinson, B. Hanna, and P. Theobald, "3d printed origami honeycombs with tailored out-of-plane energy absorption behavior," *Materials & Design*, vol. 195, p. 108930, 2020.

[7] Y. Chen, R. Peng, and Z. You, "Origami of thick panels," *Science*, vol. 349, no. 6246, pp. 396–400, 2015.

[8] S. Li, D. M. Vogt, D. Rus, and R. J. Wood, "Fluid-driven origami-inspired artificial muscles," *Proceedings of the National academy of Sciences*, vol. 114, no. 50, pp. 13 132–13 137, 2017.

[9] S. Li, J. J. Stampfli, H. J. Xu, E. Malkin, E. V. Diaz, D. Rus, and R. J. Wood, "A vacuum-driven origami "magic-ball" soft gripper," in *2019 International Conference on Robotics and Automation (ICRA)*. IEEE, 2019, pp. 7401–7408.

[10] Q. Ze, S. Wu, J. Dai, S. Leanza, G. Ikeda, P. C. Yang, G. Iaccarino, and R. R. Zhao, "Spinning-enabled wireless amphibious origami millirobot," *Nature communications*, vol. 13, no. 1, p. 3118, 2022.

[11] J. Cools, Q. Jin, E. Yoon, D. Alba Burbano, Z. Luo, D. Cuypers, G. Callewaert, D. Braeken, and D. H. Gracias, "A micropatterned multielectrode shell for 3d spatiotemporal recording from live cells," *Advanced Science*, vol. 5, no. 4, p. 1700731, 2018.

[12] A. Jamalimehr, M. Mirzajanzadeh, A. Akbarzadeh, and D. Pasini, "Rigidly flat-foldable class of lockable origami-inspired metamaterials with topological stiff states," *Nature communications*, vol. 13, no. 1, p. 1816, 2022.

[13] Y. Li, A. Di Lallo, J. Zhu, Y. Chi, H. Su, and J. Yin, "Adaptive hierarchical origami-based metastructures," *Nature Communications*, vol. 15, no. 1, p. 6247, 2024.

[14] Z. E. Teoh, B. T. Phillips, K. P. Becker, G. Whittredge, J. C. Weaver, C. Hoberman, D. F. Gruber, and R. J. Wood, "Rotary-actuated folding polyhedrons for midwater investigation of delicate marine organisms," *Science Robotics*, vol. 3, no. 20, p. eaat5276, 2018.

[15] Z. Zhang, G. Chen, H. Wu, L. Kong, and H. Wang, "A pneumatic/cable-driven hybrid linear actuator with combined structure of origami chambers and deployable mechanism," *IEEE Robotics and Automation Letters*, vol. 5, no. 2, pp. 3564–3571, 2020.

[16] P. Yang and S. Li, "Design and fabrication of string-driven origami robots," *arXiv preprint arXiv:2404.09222*, 2024.

[17] S. M. Felton, M. T. Tolley, B. Shin, C. D. Onal, E. D. Demaine, D. Rus, and R. J. Wood, "Self-folding with shape memory composites," *Soft matter*, vol. 9, no. 32, pp. 7688–7694, 2013.

[18] K. Kuribayashi, K. Tsuchiya, Z. You, D. Tomus, M. Umemoto, T. Ito, and M. Sasaki, "Self-deployable origami stent grafts as a biomedical application of ni-rich tini shape memory alloy foil," *Materials Science and Engineering: A*, vol. 419, no. 1-2, pp. 131–137, 2006.

[19] Y. Kim and X. Zhao, "Magnetic soft materials and robots," *Chemical reviews*, vol. 122, no. 5, pp. 5317–5364, 2022.

[20] J. Ou, M. Skouras, N. Vlavianos, F. Heibeck, C.-Y. Cheng, J. Peters, and H. Ishii, "aeromorph-heat-sealing inflatable shape-change materials for interaction design," in *Proceedings of the 29th Annual Symposium on User Interface Software and Technology*, 2016, pp. 121–132.

[21] S. Dontu, E. Kanhere, T. Stalin, A. G. Dharmawan, C. Hegde, J. Su, X. Chen, S. Magdassi, G. S. Soh, and P. Valdivia Y. Alvarado, "Applications of a vacuum-actuated multi-material hybrid soft gripper: lessons learnt from robosoft manipulation challenge," *Frontiers in Robotics and AI*, vol. 11, p. 1356692, 2024.

[22] J. Lewis, "Direct Ink Writing of 3D Functional Materials," *Advanced Functional Materials*, vol. 16, no. 17, pp. 2193–2204, Nov. 2006.

[23] G. Liu, Y. Zhao, G. Wu, and J. Lu, "Origami and 4d printing of elastomer-derived ceramic structures," *Science Advances*, vol. 4, no. 8, p. eaat0641, 2018.

[24] T. Stalin, A. R. Plamootil Mathai, N. K. Thanigaivel, E. Kanhere, S. Dontu, G. Hiramandala, A. Chooi, A. Castillo Ugalde, and P. Valdivia Y Alvarado, "Architected Design and Fabrication of Soft Mechanical Metamaterials," *Advanced Intelligent Systems*, p. 2400514, 2024.

[25] T. Calais, N. D. Sanandiya, S. Jain, E. V. Kanhere, S. Kumar, R. C.-H. Yeow, and P. Valdivia y Alvarado, "Freeform liquid 3d printing of soft functional components for soft robotics," *ACS Applied Materials & Interfaces*, vol. 14, no. 1, pp. 2301–2315, 2021.

[26] E. Kanhere, T. Calais, S. Jain, A. R. Plamootil Mathai, A. Chooi, T. Stalin, V. S. Joseph, and P. Valdivia y Alvarado, "Upgrading and extending the life cycle of soft robots with in situ free-form liquid three-dimensional printing," *Science Robotics*, vol. 9, no. 97, p. eadn4542, 2024.

[27] "UltiMaker Cura - Ultimaker," https://ultimaker.com/software/ultimaker-cura/, [Accessed 25-10-2024].

[28] "PrusaSlicer — Original Prusa 3D printers directly from Josef Prusa," https://www.prusa3d.com/, [Accessed 25-10-2024].

[29] "OctoPrint.org," https://octoprint.org/, [Accessed 25-10-2024].

[30] S. Felton, M. Tolley, E. Demaine, D. Rus, and R. Wood, "A method for building self-folding machines," *Science*, vol. 345, no. 6197, pp. 644–646, 2014.

[31] "Living Hinge Basics for Injection Molding — protolabs.com," https://www.protolabs.com/resources/blog/living-hinge-basics-for-injection-molding/, [Accessed 25-10-2024].

[32] B. Zhou and T. Tian, "A path planning method of lattice structural components for additive manufacturing," *The International Journal of Advanced Manufacturing Technology*, vol. 116, no. 5, pp. 1467–1490, 2021.

[33] E. Demaine and T. Tachi, "Origamizer: A practical algorithm for folding any polyhedron," 2017.

[34] L. Jin, M. Yeager, Y.-J. Lee, D. J. O'Brien, and S. Yang, "Shape-morphing into 3d curved surfaces with nacre-like composite architectures," *Science Advances*, vol. 8, no. 41, p. eabq3248, 2022.

[35] "NC Viewer // GCode Viewer and Machine Simulator," https://ncviewer.com/, [Accessed 25-10-2024].

[36] J.-s. Koh, S.-r. Kim, and K.-j. Cho, "Self-folding origami using torsion shape memory alloy wire actuators," in *International Design Engineering Technical Conferences and Computers and Information in Engineering Conference*, vol. 46377. American Society of Mechanical Engineers, 2014, p. V05BT08A043.